

Crystallization processes and magnetic properties of $\text{Fe}_{78}\text{Co}_2\text{Zr}_8\text{Nb}_2\text{B}_{10-x}\text{Ge}_x$ ($x = 0, 1, 2, 3$) amorphous alloys

Z. Hua^{*,†}, B. Zuo^{*}, Y. M. Sun^{*}, X. N. Wang^{*}, L. R. Dong^{*} and B. Li[†]

^{*}Key Laboratory of Functional Materials Physics and Chemistry of the Ministry of Education,
Jilin Normal University, Siping 136000, China

[†]Changchun Institute of Optics, Fine Mechanics and Physics,
Chinese Academy of Sciences, Dong Nanhu Road 3888, Changchun 130012, China
‡huazhong196110@163.com

Received 8 January 2014

Revised 30 May 2014

Accepted 23 June 2014

Published 10 August 2014

$\text{Fe}_{78}\text{Co}_2\text{Zr}_8\text{Nb}_2\text{B}_{10-x}\text{Ge}_x$ ($x = 0, 1, 2, 3$) amorphous alloys were prepared by melt-spinning and annealed at different temperatures. The microstructures and magnetic property were investigated by X-ray diffraction (XRD), transmission electron microscopy (TEM) and vibrating sample magnetometer (VSM), respectively. The crystallization processes of $\text{Fe}_{78}\text{Co}_2\text{Zr}_8\text{Nb}_2\text{B}_{10}$ amorphous alloy at different quenching rates are similar and complex. The α -Fe(Co) and α -Mn type phases are observed in their initial stage of crystallization process. H_c increases with increasing annealing temperature in general. Only α -Fe(Co) phase is observed in the initial stage of the crystallization processes of $\text{Fe}_{78}\text{Co}_2\text{Zr}_8\text{Nb}_2\text{B}_{10-x}\text{Ge}_x$ ($x = 0, 1, 2, 3$) alloys. The change trend of coercivity is complex compared with Ge-free samples. The magnetic property of $\text{Fe}_{78}\text{Co}_2\text{Zr}_8\text{Nb}_2\text{B}_7\text{Ge}_3$ is better.

Keywords: Quenching rate; crystallization process; microstructure.

1. Introduction

Fe-based nanocrystalline alloys have attracted a great deal of attention from scientists over the past several decades due to their excellent soft magnetic properties. Among the Fe-based soft magnetic nanocrystalline systems, considerable attention is devoted to the Fe–M–B type alloys (where M = Zr, Hf and Nb).^{1–3} The crystallization processes of Fe–M–B type alloys have been reported extensively. While the formation of crystalline phases in devitrified amorphous Fe–Zr–B alloys is still being debated.⁴ The devitrification process of amorphous alloy is affected by adding alloy chemistry. Besides the α -Fe phase has been confirmed in devitrified amorphous Fe–Zr–B based alloys,⁵ the formations of $\text{Fe}_{23}\text{Zr}_6$,⁴ α -Mn type⁶ and H-phase⁷ crystalline phases have been reported.

Suzuki⁸ showed that the addition of Ge element improved the Curie temperature of FeZrBCu alloy. Sun⁹ reported that the addition of Ge element stabled the residual amorphous phase of FeCoZrB alloys, inhibited the growth of the grain size as well as to reduce the high temperature coercivity. In this paper, Fe₇₈Co₂Zr₈Nb₂B_{10-x}Ge_x ($x = 0, 1, 2, 3$) amorphous alloys were prepared. The crystallization processes and magnetic properties of Fe₇₈Co₂Zr₈Nb₂B_{10-x}Ge_x ($x = 0, 1, 2, 3$) amorphous alloys were studied.

2. Experimental Details

Fe₇₈Co₂Zr₈Nb₂B₁₀ alloys prepared using single roller melt-spinning equipment with copper wheel rotating at surface velocities of 32, 36 and 38 m/s. Fe₇₈Co₂Zr₈Nb₂B_{10-x}Ge_x ($x = 1, 2, 3$) alloys were prepared at a surface velocity of 38 m/s. The amorphous alloys were annealed at 500, 525, 550, 575, 600, 625, 650, 700, 750 and 800°C for 1 h. Structural characterizations of samples were examined by X-ray diffraction (XRD, D/max 2500/PC, Cu-K α , $\lambda = 1.5406 \text{ \AA}$) and transmission electron microscopy (TEM, JEM-2100E). The grain size is calculated by Scherrer formula $D = 0.89\lambda/\beta \cos \theta$ (β indicates the width of half-height diffraction peak, θ is Bragg angle, λ is X-ray wavelength, D is grain size). The magnetic property was performed by the vibrating sample magnetometer (VSM, Lake Shore M-7407).

3. Results and Discussion

Figure 1 shows the XRD patterns of Fe₇₈Co₂Zr₈Nb₂B₁₀ alloys at different quenching rates for different annealing temperatures.

No crystalline peaks are observed in the XRD patterns of the three alloys as-quenched. After annealing above 575°C, some crystalline phases precipitate from the amorphous matrix. Further increase of annealing temperature leads to the increase of the intensity of crystalline phases. The crystallization processes of Fe₇₈Co₂Zr₈Nb₂B₁₀ amorphous alloys at different quenching rates are similar, complex and interesting.

In order to investigate the crystallization process more clearly, XRD patterns of alloy at a quenching rate of 32 m/s ranging from 575°C to 800°C were shown in Fig. 2. The α -Fe(Co) and α -Mn type phases are observed in the initial stage of crystallization process. The peaks of another phase at about 38°, 41°, 45° and 48° are observed at higher temperature, which is defined as λ phase reported by Lyasotskii *et al.*¹⁰ The α -Mn type phase and λ phase disappear gradually with increasing annealing temperature. The λ phase is another metastable phase in devitrified amorphous Fe-Zr-B based alloy besides α -Mn type⁶ and H-phase⁷ reported by us.

Figure 3 shows M_s and H_c of Fe₇₈Co₂Zr₈Nb₂B₁₀ alloys at different quenching rates as a function of annealing temperature (T_a). Both M_s and H_c of three alloys

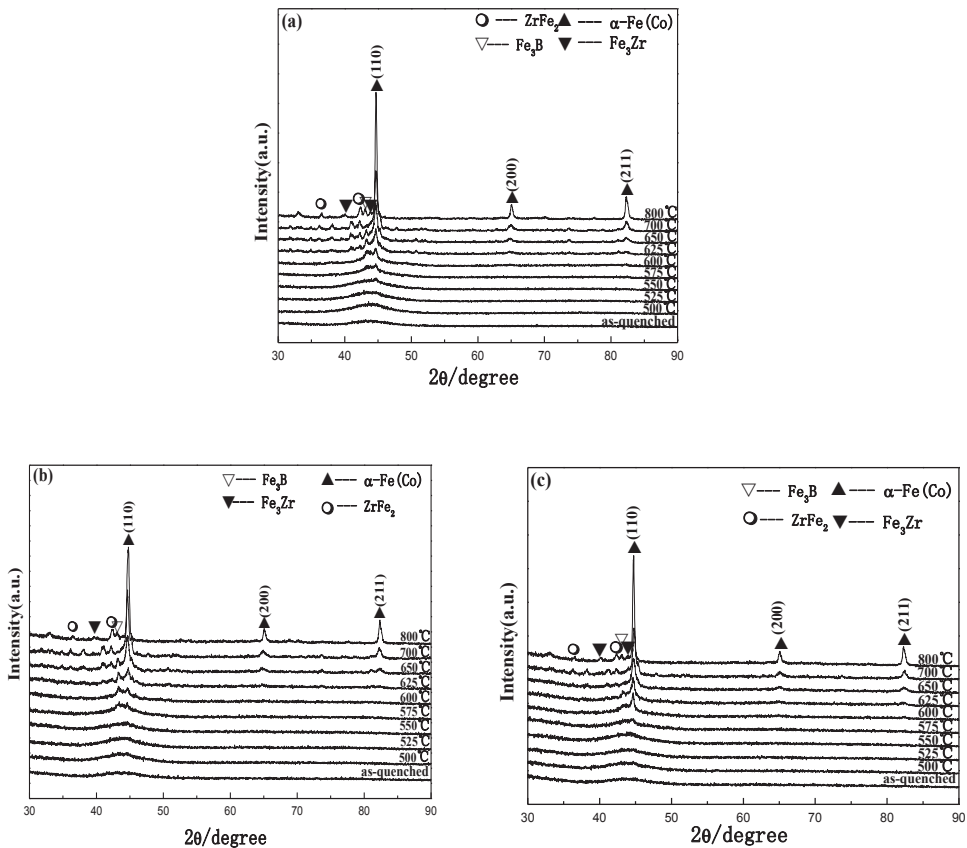


Fig. 1. XRD patterns of Fe₇₈Co₂Zr₈Nb₂B₁₀ alloys at different quenching rates for different annealing temperatures (a) 32 m/s, (b) 36 m/s and (c) 38 m/s.

increase with increasing annealing temperature in general. Due to the precipitation of intermetallic compounds, H_c of the three alloys are all large above 575°C.

In comparison, Fe₇₈Co₂Zr₈Nb₂B₁₀ alloy at high quenching rate has high M_s and low H_c . Therefore, Fe₇₈Co₂Zr₈Nb₂B_{10-x}Ge_x ($x = 1, 2, 3$) amorphous alloys were prepared at a high quenching rate (38 m/s).

XRD patterns of Fe₇₈Co₂Zr₈Nb₂B_{10-x}Ge_x ($x = 1, 2, 3$) amorphous alloys as-quenched and annealed at different annealing temperatures are shown in Fig. 4. The three alloys as-quenched all form amorphous. After annealing at 575°C, the alloy starts to crystallize into α -Fe(Co) phase and no other phases are detected below 700°C in Fe₇₈Co₂Zr₈Nb₂B₉Ge₁ alloy. The Ge doping simplifies the process of crystallization of Fe₇₈Co₂Zr₈Nb₂B₁₀ alloy. With increasing annealing temperature, the diffraction peak intensity of α -Fe(Co) increases gradually. The Fe₃Zr and Fe₂B phases are observed at the final crystallization stage. The crystallization processes of Fe₇₈Co₂Zr₈Nb₂B_{10-x}Ge_x ($x = 1, 2, 3$) alloys are similar. The difference is that the

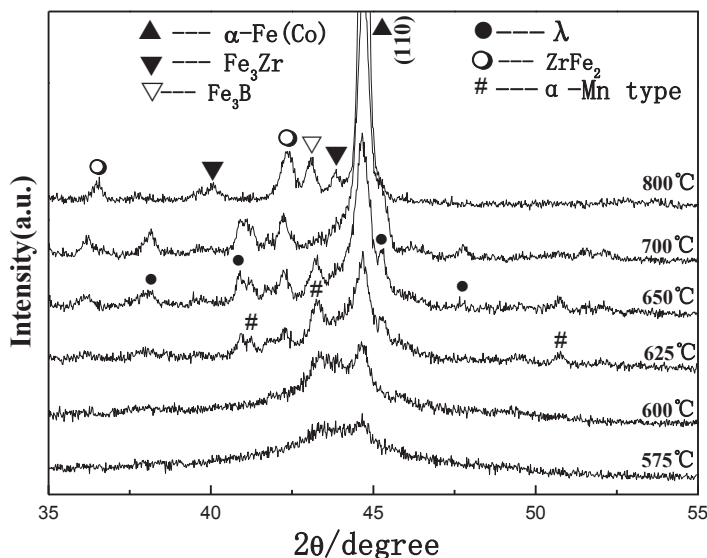


Fig. 2. XRD patterns of $\text{Fe}_{78}\text{Co}_2\text{Zr}_8\text{Nb}_2\text{B}_{10}$ alloy at a quenching rate of 32 m/s ranging from 575°C to 800°C.

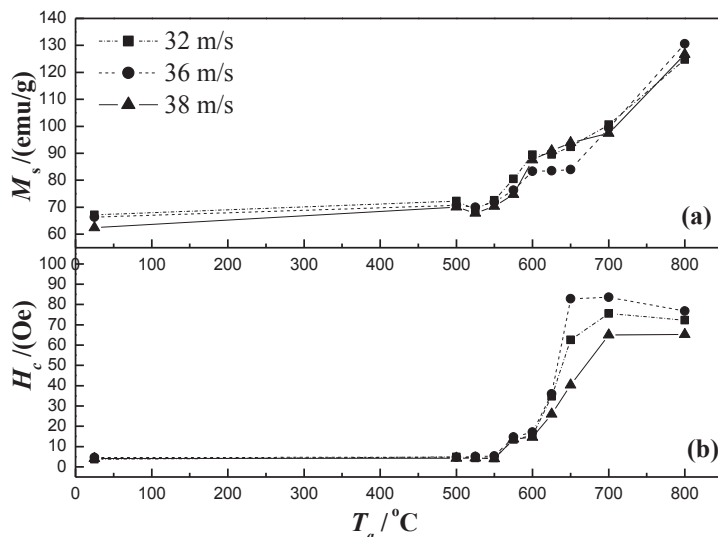


Fig. 3. M_s (a) and H_c (b) of $\text{Fe}_{78}\text{Co}_2\text{Zr}_8\text{Nb}_2\text{B}_{10}$ alloys at different quenching rates as a function of annealing temperature (T_a).

$\alpha\text{-Fe(Co)}$ phase already precipitates in the $\text{Fe}_{78}\text{Co}_2\text{Zr}_8\text{Nb}_2\text{B}_7\text{Ge}_3$ alloy annealed at 550°C. That is to say, the increase of Ge content promotes the nucleation of $\alpha\text{-Fe(Co)}$ phase.

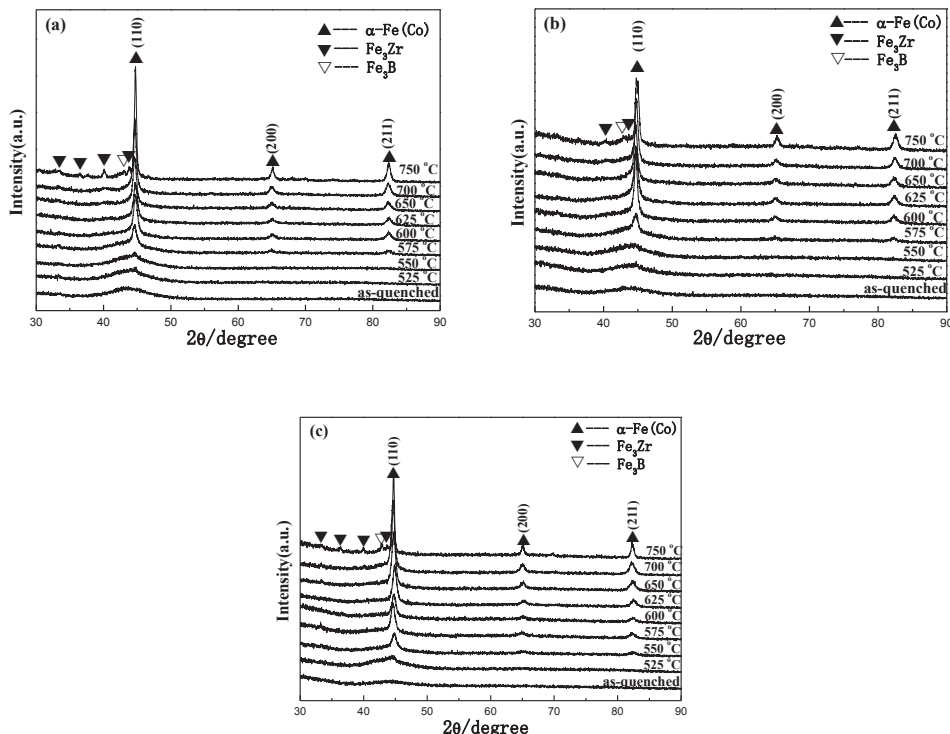


Fig. 4. XRD patterns of $\text{Fe}_{78}\text{Co}_2\text{Zr}_8\text{Nb}_2\text{B}_{10-x}\text{Ge}_x$ ($x = 1, 2, 3$) amorphous alloys as-quenched and annealed at different annealing temperatures. (a) $\text{Fe}_{78}\text{Co}_2\text{Zr}_8\text{Nb}_2\text{B}_9\text{Ge}_1$, (b) $\text{Fe}_{78}\text{Co}_2\text{Zr}_8\text{Nb}_2\text{B}_8\text{Ge}_2$ and (c) $\text{Fe}_{78}\text{Co}_2\text{Zr}_8\text{Nb}_2\text{B}_7\text{Ge}_3$.

Table 1. The crystallite size of α -Fe(Co) phase of $\text{Fe}_{78}\text{Co}_2\text{Zr}_8\text{Nb}_2\text{B}_{9-x}\text{Ge}_x$ ($x = 1, 2, 3$) amorphous alloys annealed at different annealing temperatures.

	550°C	575°C	600°C	625°C	650°C	700°C	750°C
$\text{Fe}_{78}\text{Co}_2\text{Zr}_8\text{Nb}_2\text{B}_9\text{Ge}_1$	—	11.2	11.9	13.0	15.7	17.1	30.8
$\text{Fe}_{78}\text{Co}_2\text{Zr}_8\text{Nb}_2\text{B}_8\text{Ge}_2$	—	11.7	12.5	13.3	15.9	17.4	25.3
$\text{Fe}_{78}\text{Co}_2\text{Zr}_8\text{Nb}_2\text{B}_7\text{Ge}_3$	9.6	12.2	12.9	13.5	17.6	18.9	34.9

Table 1 shows the crystallite size of α -Fe(Co) phase of $\text{Fe}_{78}\text{Co}_2\text{Zr}_8\text{Nb}_2\text{B}_{10-x}\text{Ge}_x$ ($x = 1, 2, 3$) amorphous alloys annealed at different annealing temperatures. The crystallite size of three alloys all increases gradually with increasing annealing temperature and keeps at the nanoscale.

Figure 5 shows M_s and H_c of $\text{Fe}_{78}\text{Co}_2\text{Zr}_8\text{Nb}_2\text{B}_{10-x}\text{Ge}_x$ ($x = 1, 2, 3$) alloys as a function of annealing temperature (T_a).

M_s of $\text{Fe}_{78}\text{Co}_2\text{Zr}_8\text{Nb}_2\text{B}_{10-x}\text{Ge}_x$ ($x = 1, 2, 3$) alloys are similar as a function of annealing temperature. Above 550°C, M_s increases gradually with the increase of α -Fe(Co) phases from the amorphous matrix. Above 525°C, H_c increases first

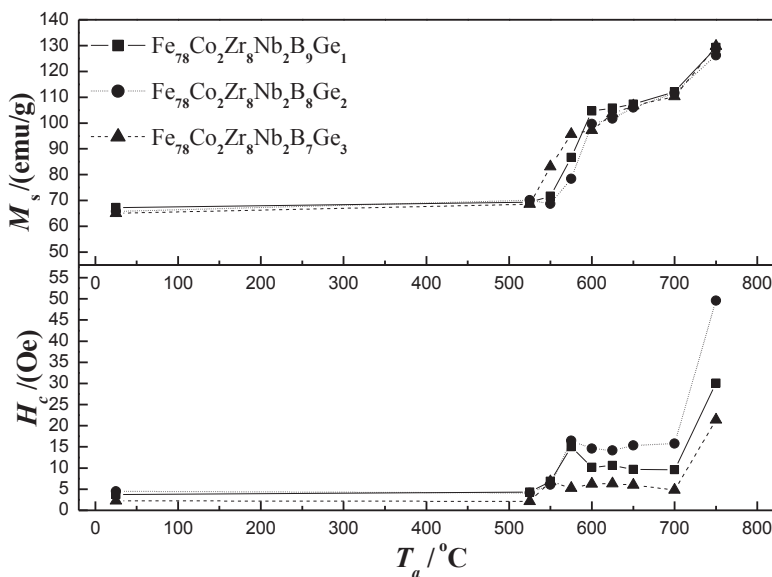


Fig. 5. M_s and H_c of $\text{Fe}_{78}\text{Co}_2\text{Zr}_8\text{Nb}_2\text{B}_{10-x}\text{Ge}_x$ ($x = 1, 2, 3$) alloys as a function of annealing temperature (T_a).

and then decreases, and increases at last. By comparing Fig. 5 and Fig. 2, we can see that the coercivity lines are completely different. The coercivity is not a monotonous function of the annealing temperature. The deterioration in H_c at the beginning of the crystallization process is detected. The magnetic property of $\text{Fe}_{78}\text{Co}_2\text{Zr}_8\text{Nb}_2\text{B}_7\text{Ge}_3$ is better.

TEM images and the corresponding selected area diffraction pattern for $\text{Fe}_{78}\text{Co}_2\text{Zr}_8\text{Nb}_2\text{B}_9\text{Ge}_1$ alloy annealed at 575°C are shown in Figs. 6(a) and 6(a'), and annealed at 625°C is shown in Fig. 6(b). The TEM image, the corresponding selected area diffraction pattern and grain size distribution profile for $\text{Fe}_{78}\text{Co}_2\text{Zr}_8\text{Nb}_2\text{B}_7\text{Ge}_3$ alloy annealed at 575°C are shown in Figs. 6(c) and 6(d).

From SADP of $\text{Fe}_{78}\text{Co}_2\text{Zr}_8\text{Nb}_2\text{B}_9\text{Ge}_1$ alloy [Fig. 6(a)] and $\text{Fe}_{78}\text{Co}_2\text{Zr}_8\text{Nb}_2\text{B}_8\text{Ge}_3$ alloy [Fig. 6(c)], only the $\alpha\text{-Fe}(\text{Co})$ phase is observed. However, the morphologies of two alloys are different. The amplified TEM image [Fig. 6(a')] of $\text{Fe}_{78}\text{Co}_2\text{Zr}_8\text{Nb}_2\text{B}_9\text{Ge}_1$ alloy shows irregular aggregates of grains, not the “finemet”-like structure. The special morphology results in the weak magnetic matrix between nanocrystalline grains, so H_c deteriorates at the beginning of the crystallization process. The observed magnetic softening later is attributed to the increase of $\alpha\text{-Fe}(\text{Co})$ phase [Fig. 6(b)]. For $\text{Fe}_{78}\text{Co}_2\text{Zr}_8\text{Nb}_2\text{B}_8\text{Ge}_3$ alloy the $\alpha\text{-Fe}(\text{Co})$ nanocrystallites embed in residual amorphous phase like “finemet” structure. The mean grain size from grain size distribution profile is about 11.8 nm, which is close to the grain size calculated by Scherrer's formula (12.2 nm). The soft magnetic characterization arises from the presence of intergranular magnetic coupling between adjacent

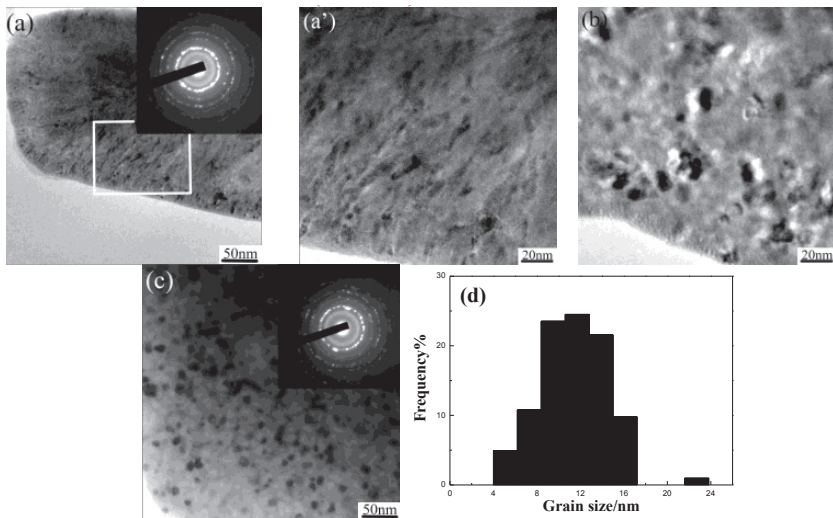


Fig. 6. TEM image and the corresponding selected area diffraction pattern (SADP) for $\text{Fe}_{78}\text{Co}_{2}\text{Zr}_{8}\text{Nb}_{2}\text{B}_{9}\text{Ge}_{1}$ alloy annealed at 575°C (a), the amplified TEM image of the indicated area (a'), TEM image of $\text{Fe}_{78}\text{Co}_{2}\text{Zr}_{8}\text{Nb}_{2}\text{B}_{9}\text{Ge}_{1}$ alloy annealed at 625°C (b), TEM image and the corresponding selected area diffraction pattern (SADP) for $\text{Fe}_{78}\text{Co}_{2}\text{Zr}_{8}\text{Nb}_{2}\text{B}_{7}\text{Ge}_{3}$ alloy annealed at 575°C (c), grain size distribution profile (d).

nanocrystals through the residual amorphous phase. The rapid increase in the H_c of three alloys observed at 750°C is assumed to the precipitation of Fe_3Zr and Fe_2B phases.

4. Conclusion

- (i) The crystallization processes of $\text{Fe}_{78}\text{Co}_{2}\text{Zr}_{8}\text{Nb}_{2}\text{B}_{10}$ amorphous alloys with different quenching rates are similar and complex. The $\alpha\text{-Fe}(\text{Co})$ and $\alpha\text{-Mn}$ type phases are observed in their initial stage of crystallization process. Both M_s and H_c of alloys increase with the increasing of annealing temperature.
- (ii) The crystallization processes of $\text{Fe}_{78}\text{Co}_{2}\text{Zr}_{8}\text{Nb}_{2}\text{B}_{10-x}\text{Ge}_x$ ($x = 1, 2, 3$) alloys are similar. Only $\alpha\text{-Fe}(\text{Co})$ phase is observed in their initial stage of the crystallization process. M_s of three alloys increase with the increasing of annealing temperature. The change trend of H_c is complex. A decrease of H_c is observed at 600°C in $\text{Fe}_{78}\text{Co}_{2}\text{Zr}_{8}\text{Nb}_{2}\text{B}_{10-x}\text{Ge}_x$ ($x = 1, 2$) alloys. The magnetic property of $\text{Fe}_{78}\text{Co}_{2}\text{Zr}_{8}\text{Nb}_{2}\text{B}_7\text{Ge}_3$ is better.

Acknowledgments

This work was funded by Science and Technology Development Project of Jilin Province (No. 201105083), Science and Technology Studying Project of “12th five-year” Office of Education of Jilin Province (No. 2014-485) and Graduate Innovative Research Programs of Jilin Normal University (No. 201103).

References

1. D. Arvindha Babu, B. Majumdar, R. Sarkar, D. Akhtar and V. Chandrasekaran, *J. Mater. Res.* **16** (2011) 2065.
2. K. Shen, M. P. Wang, L. F. Cao, M. X. Guo, S. M. Li and Q. Y. Dong, *Chin. J. Nonferrous Metals* **17** (2007) 1661.
3. K. Suzuki, A. Makino, A. Inoue and T. Masumoto, *J. Appl. Phys.* **70** (1991) 6232.
4. H. Huang, G. Shao and P. Tsakiroopoulos, *J. Alloys Compd.* **459** (2008) 185.
5. Z. Hua, Y. M. Sun, W. Q. Yu and M. B. Wei, *Int. J. Mod. Phys. B* **26** (2012) 1250088.
6. W. Q. Yu, Y. M. Sun and Z. Hua, *Appl. Surf. Sci.* **257** (2011) 9733.
7. W. Q. Yu, X. C. Meng, B. Zuo, Y. M. Sun, B. Li and Z. Hua, *Int. J. Mod. Phys. B* **28** (2014) 1450083.
8. K. Suzuki, J. W. Cochrane, J. M. Cadogan, X. Y. Xiong and K. Hono, *J. Appl. Phys.* **91** (2002) 8417.
9. Y. Sun, L. Zhong and X. F. Bi, *Scripta Mater.* **60** (2009) 814.
10. I. V. Lyasotskii, N. B. Dyakonova, E. N. Vlasova, D. L. Dyakonov and M. Yu. Yazvitskii, *Phys. Status Solidi A* **203** (2006) 259.